Fine and ultrafine particle deposition in packed-bed catalytic reactors

Fine and ultrafine particle deposition in packed-bed catalytic reactors

Gianluca Boccardo[a,*], Rajandrea Sethi[b], Daniele L. Marchisio[a]

[a] *Department of Applied Science and Technology, Politecnico di Torino, Italy*
[b] *Department of Environment, Land and Infrastructure Engineering, Politecnico di Torino, Italy*

Abstract

In this work we have performed an extensive CFD simulation campaign with the purpose of studying particle transport and deposition in different catalytic systems and under different conditions. Two types of geometric models representing different porous media were created. The first is a number of random packings of spheres created via rigid body simulations: this approach was tested in previous studies and was proved to result in realistic packings, validated in their geometric features and fluid dynamic behaviour. The second is a regular arrangement of spheres, which was also successfully employed in previous works to study fine particles dispersion.

Using these random packings, simulations of particle deposition have been performed at different operating conditions. In the first part we calculated values of particle deposition efficiency and compared our results with the classical filtration theory, highlighting the criticalities in the use of the simplified models upon which the theory is based. In the second part we have studied the effect of polydisperse particle populations: this is also missing in the classical filtration theory, which always considers the transport of particles with uniform diameter. Thus, we have performed population balance modelling simulations for particle deposition, employing the quadrature method of moments (QMOM): as an accompanying technical addition, a study on the accuracy of the application of EQMOM in these systems is offered. Even more clearly in this case, the results show that the description of polydisperse populations has a very noticeable effect on the macro-scale description, which would dramatically improve the understanding of particle transport and deposition in filtration and catalytic processes.

Keywords: catalytic reactors, filtration, particle deposition, `Blender`, `OpenFOAM`, QMOM

*Corresponding author

1. Introduction

Catalytic reactors are of central importance in chemical engineering, as they represent one of the two main steps in virtually any process, together with product separation. The process of filtration, especially relevant to the latter, is also strictly connected to catalytic processes, especially in automotive applications regarding catalytic [1] and particulate filters [2, 3, 4], or in other systems as a downstream [5] or separate unit operation [6]. For the most part, the study of a filtration or catalytic process deals with treating a geometrical system where there is a discernible microstructure, which could be an arranged (regular) or random medium. Both types have been studied extensively: random media can be granular bed reactors [7, 8, 9], or catalytic foams [10, 11, 12]; structured porous media are also being studied [13, 14]. The detailed study of the small-scale physics in structured reactors is also becoming very important in the investigation of transport of a dispersed phase (e.g.: bubbles) in multiphase systems [15, 16, 17]

The presence of this microstructure makes the study of these systems, and porous media in general, an inherent multi-scale problem, presenting a challenge in the connection of the models relevant to both scales. The problem is compounded by the manifest difficulty in the experimental investigation of these systems, especially at the scale of the pore: in-depth observations are very difficult when not outright impossible, and yet it is transport phenomena taking place at the micro-scale having the greatest impact on the systems macroscopic (e.g.: reactor-scale) behaviour. The employed modelling simplifications have usually involved sweeping assumptions in the structure of fluid flow in the reactors. In the case of filtration, as it will be described in the next section, the classical models which are still used as a relevant modelling reference propose a very simplified description of the structure of a porous medium. In this context, the necessity of detailed mathematical modelling of both fluid flow and mass transport at the pore-scale, and the relation of these results to the relevant macroscopic scale through an upscaling procedure, becomes clear.

For this reason, in this work we have performed an extensive computational study, composed of several distinct simulation campaigns, each tackling a different aspect in which the classical descriptions are lacking. First we present the method by which we generated our random packings, which has been proven to result in realistic and validated geometric structures. To ensure the accuracy of the proposed CFD results, a study regarding the technical and conceptual aspects of the simulation was performed: informations regarding the grid convergence of the results are offered together with an analysis of the correct representative elementary volume (REV) for the phenomena under study. Then, we performed simulations on both random and structured porous media. In the first case we have studied filtration of particles in their different deposition mechanisms and compared our results with the theoretical predictions, highlighting the issues with the constitutive equations obtained by the classical description. Then, we approached the investigation of the transport and deposition of polydisperse particles, which is completely missing from the available

filtration laws. Especially in this case the results put in evidence how correctly tracking the transport of a realistic polydisperse population dramatically improves the description of its evolution, and has a great effect on the description of the system at the macroscopic scale.

2. Governing equations

2.1. Physical description at the scale of the pore

As introduced at the beginning of the manuscript, the objective of this work is to obtain a close understanding of the physical behaviour of the system by a *first-principles* approach: in the case of packed beds and porous media in general, this means obtaining the solution to the relevant transport equation at the scale of the medium pores. As such, the first step is the solution of the Navier-Stokes equations,

$$\begin{aligned} \rho \mathbf{u} \cdot \nabla \mathbf{u} &= -\nabla p + \mu \nabla^2 \mathbf{u} \\ \nabla \cdot \mathbf{u} &= 0 \, , \end{aligned} \tag{1}$$

where ρ is the density of the fluid (kg m^{-3}), $\mathbf{u}$ is the effective velocity (m s^{-1}), p is the pressure (kg m^{-1} s^{-2}), and μ is the fluid dynamic viscosity (kg m^{-1} s^{-1}). The relevant dimensionless number is the Reynolds number, where the characteristic length is taken to be equal to the average diameter of the grains constituting the packed bed D_g, so $\mathrm{Re} = \rho U D_g / \mu$. The characteristic velocity U is instead simply the superficial velocity, calculated as $U = u\varepsilon$ [1], where ε is the packed bed porosity.

In this work we want to investigate the transport and deposition of fine and ultra-fine species, and when modelling suspensions of colloidal or at most micron-sized particles, it is possible to work under the hypothesis of one-way coupling, which is to assume that the particles motion follows the fluid streamlines without affecting it in kind. As such, we represent the particles in an Eulerian framework as a scalar quantity, namely their concentration in the fluid phase, c (mol m^{-3}). To obtain this quantity, using the flow field obtained from the solution of Eq.1, the classical advection-diffusion equation is solved, which reads

$$\frac{\partial c}{\partial t} + \mathbf{u} \cdot \nabla c = \mathcal{D} \nabla^2 c \, . \tag{2}$$

Here, the coefficient $\mathcal{D}$ is the particles molecular diffusion coefficient (m^2 s^{-1}), which was obtained via the well known Stokes-Einstein equation as $\mathcal{D} = k_B T / (3\pi\mu d_p)$, where d_p is the dispersed particle diameter (m), T the fluid temperature (K), and k_B the Boltzmann constant (m^2 kg s^{-2} K^{-1}); it has to be noted that the systems

[1] Also, the scalar quantity u is the volume integral of the x-component of $\mathbf{u}$, taking x to be the main flow direction.

under consideration are isothermal, and T is thus constant in space. The dimensionless Péclet number describing mass transport is given by $\mathrm{Pe} = D_g U/\mathcal{D}$. To study the effect of particle sedimentation on their transport and deposition, a simple modification of Eq. 2 was employed, by adding to its advective term the settling velocity of the monodisperse particle population considered. For particles of diameter d_p, it reads:

$$U_{sed} = \frac{\mathbf{g} d_p^2 (\rho_s - \rho_f)}{18\mu} \ , \tag{3}$$

where $\mathbf{g}$ is the gravitational acceleration (m s^{-2}) and the subscripts of the density terms refer to solid particles and fluid, respectively.

In the second part of this work instead, we studied the transport of polydisperse particles, with the objective of describing the evolution of the particle size distribution, and the possible effect on deposition efficiency, which will be compared to the monodisperse case. The dispersed particle population in our case can be described by a univariate population balance equation, which reads:

$$\frac{\partial n(d_p)}{\partial t} + \nabla \cdot (\mathbf{u}\ n(d_p)) = \nabla \cdot (\mathcal{D} \nabla n(d_p)) \ . \tag{4}$$

In this balance equation, the transported quantity $n(d_p)$ is the number density function representing the distribution of the quantity of particles, depending only on their size d_p. It has to be noted that in this initial work we wanted to consider a simplified form of the population balance equation. The terms related to possible particle aggregation or breakage are missing, and Eq. 4 in its current form represents instead a direct parallel of the Eq. 2, comprising only the advective and diffusive contributions; the study of first- and second-order processes (e.g.: breakage of aggregates, or their formation) will be treated in future works. The solution of the population balance equation was implemented in the CFD code by integrating it and obtaining a transport equation for the statistical moments of k-th order of the distribution, m_k, which reads:

$$\frac{\partial m_k}{\partial t} + \nabla \cdot (\mathbf{u}_f m_k) = \Gamma_0 \nabla^2 m_{k-1} \ , \tag{5}$$

where the new diffusive coefficient $\Gamma_0 = k_B T/(3\pi\mu)$. The implementation and solution of Eq. 5 in the CFD code is done via the quadrature-based method of moments (QMOM), which is based on a functional expression of the particle distribution $n(d_p)$ given by a summation of delta functions centered on suitable nodes of a Gaussian quadrature approximation. Using a modified version of this method called EQMOM (as in *extended* QMOM [18, 19]), it is possible to reconstruct a smooth number density function, at the cost of the solution of one additional moment equation with respect to the simple QMOM[2]. For

[2]It must be noted that the use of this method carries a number of practical caveats which means it is not applicable *a priori* in every system: we devote Appendix A to an expansive analysis of the numerical accuracy in the use of EQMOM for the systems under investigation

the interested reader, we refer to the detailed and in-depth explanation of the theory of the method of moments and of these computational techniques found in [20]. Perhaps, the most important point to note for a conscious interpretation of the results is that no reconstruction method is guaranteed to return the exact distribution to an arbitrary degree of accuracy. The EQMOM specifically, given a set of N quadrature nodes employed, will at most return a smooth and continuous distribution possessing the same $2N + 1$ first moments: however, this still represents a noticeable advantage in the cases where an analyisis of the full density function is valuable, as is the present one. Moreover, it has to be noted that this is not the only method which can be used for the purpose of reconstructing the number density function and, depending on the case, other methods may be more appropriate. For example, methods based on higher order polynomial reconstruction [21] or on the maximization of the Shannon entropy [22] are also widely used. In this work we used the EQMOM only as a final post-processing step, to reconstruct the shape of the distribution found at the outlet of the computational domain and compare it to the the injected particle distribution, with the objective of calculating the deposition efficiency η, which is the upscaled parameter employable in reactor-scale equations which we obtain from the simulations pore-scale results, as it will be explained in the next section.

2.2. Upscaling pore-scale results

The equation expressing the transport and reaction of particles at the macroscopic scale is the following (for simplicity, expressed in 1D):

$$\frac{\partial \tilde{C}}{\partial t} + U\frac{\partial \tilde{C}}{\partial x}(D\frac{\partial \tilde{C}}{\partial x}) - k_d\tilde{C}\ , \tag{6}$$

where $\tilde{C}$ is the macroscale concentration and k_d is the reaction rate coefficient. In this work we will refer to the framework regarding particle filtration, which describes fine particles deposition in packed beds (and porous media in general), as was already done in other works dealing with fines deposition [3, 4], and for which an established theoretical foundation exists [23, 24]. Particle deposition in a porous medium, usually studied under the assumption of *clean-bed filtration* (i.e.: the first phase of filtration activity, before cake formation) is treated as a sequence of two steps. First, the dispersed particles are transported from the bulk of the carrying fluid to the surface of the solid grain (often called a *collector*), and this is quantified by the particle deposition efficiency η_0:

$$\eta_0 = \frac{I}{U\ C_0\frac{\pi D_g^2}{4}} \tag{7}$$

where C_0 is the bulk particle concentration and U the fluid velocity approaching the collector, and I indicates the total molar flux toward the collector. Then,

in this work.

another phenomenon has to take place on the surface of the grain, at the spatial scale of the dispersed particle: particle attachment. This depends on the physico-chemical conditions of the fluid and collector surface, affecting the balance between the repulsive and attractive forces between the particle and the solid grain; this balance is usually quantified by the attachment efficiency α which represents the probability of a particle of undergoing successful attachment (or conversely being repulsed), and whose value $0 < \alpha \leq 1$ [25, 26]. The total collector efficiency $\eta = \eta_0 \alpha$ is the product of these two factors, and using the simplifying assumption of clean bed filtration, meaning an unitary probability for particle attachment, this is reduced to $\eta = \eta_0$. Thus, it is possible to relate the quantity η_0, linked to pore-scale physics and thus obtainable from micro-scale simulations, to the macroscopic parameter k_d, in this way [27]:

$$k_d = \frac{3}{2} \frac{U}{D_g} \frac{1-\varepsilon}{\varepsilon} \eta_0 \ . \tag{8}$$

In our work, we will use a modified form of this relation to obtain the value of deposition efficiency from the results of our CFD simulations, in the form of particle concentration values at the outlet of the domain, which reads:[3]

$$\eta_0 = \frac{ln\left(\frac{C}{C_0}\right)}{-\frac{3}{2}\frac{1-\varepsilon}{\varepsilon}\frac{L}{D_g}} \ , \tag{9}$$

where L is the total length of the computational domain. Also, a simplificative assumption has been made, to consider predominance of advective flow over diffusion phenomena in the total mass transport, meaning that this relation is only valid for cases where the system's Péclet number is greater than a certain value (≈70 [28]), which represent the majority of the applications of interest. More details about this derivation, omitted here for brevity, can be found in the mentioned work by Logan [27]. It has to be mentioned that this classical expression for the calculation of deposition efficiency has been shown to be lacking in certain limiting cases[29, 30]. For example, both the case of low Péclet numbers, or equivalently the need for a very large computational domain (to describe large scale heterogeneities in the porous medium) could result in an outflow concentration very close to zero: this results in a conceptual and practical mismatch between the length of the computational domain and the length of the *active* filter, which the quantity L should represent in Eq. (9), leading to estimations of η greater than one, which clearly conflicts with its defintion as an efficiency. Recent works have proposed solutions to these problems, formulating a more robust upscaling procedure [31] to which we remand the reader for a deeper overview of the issues involved in the defition of η and its calculation

[3] Whereas in the case of the polydisperse particles simulations, the complete particle size distribution curves at the inlet and outlet (the latter reconstructed with the EQMOM as described earlier) where used in lieu of C_0 and C.

from micro-scale CFD simulations. In the cases under investigation in this work, its application is still justified, leading to realistic results.

Then, the deposition process is itself conceptually subdivided in the three different mechanisms by which particles may reach the surface of the filter solid grains. The first is Brownian diffusion, as particles may collide with the collectors due to the random motions to which they are subjected: this is the dominant mechanism in the case of sub-micron sized particles. Then, particles with a density larger than that of the carrying fluid may deposit by sedimentation, which is driven by the gravitational acceleration. Lastly, during their motion particles may also collide with the solid grains via steric interception, due to their finite size: this is relevant only for larger particles (i.e.: more then 1 μm). For this reason, we will not consider this last mechanism in the present study, and we will deal only with transport and deposition of fine and ultrafine particles. As mentioned earlier, a number of theoretical models exist for the prediction of deposition efficiency for a single considered mechanism: namely, for those relevant in our study, Browian deposition efficiency η_B and sedimentation efficiency η_G. These constituive equations are based on theoretical models first proposed by Levich [28], and further modified following studies by Happel [32]. For brevity, we will not go into the detail of their derivation here: we refer the reader to the seminal works by Yao considering all the different deposition mechanisms [33, 34], and other more recent studies based on these models [35, 36, 37, 38, 39, 40, 41]. An important point to note is that these theoretical predictions are based on very simplified geometric models: Yao's model describes a single spherical collector immersed in an unbounded fluid domain in creeping flow, where successive corrections involving Happel's studies involve an estimation of the influence of other neighboring grains on the collector itself. Moreover, the depositing particles considered are always of uniform diameter. The case of Brownian efficiency η_B, based on the Smoluchowski-Levich approximation, results in the equation:

$$\eta_B = 4.04 As^{1/3} Pe^{-2/3} \,, \tag{10}$$

where As is a parameter dependent on the medium porosity. The sedimentation efficiency instead is calculated with a simple relation:

$$\eta_G = \frac{U_{sed}}{U} = N_G \,, \tag{11}$$

where the ratio between the particles sedimentation velocity and the fluid superficial velocity is historically called the *gravity number*, N_G.

3. Numerical details and results

In this section we will present all the relevant numerical details of the simulations we performed. We start from the creation of the two chosen geometric models for the representation of porous media, then in each of the following

sections the results obtained for each explored case are presented, with an accompanying description of the relative operating conditions. For an extended treatment of the appropriateness and accuracy of using the EQMOM for the analysis of deposition efficiency results for the case of a polydisperse population, as discussed in the previous section, we refer the reader to Appendix A.

3.1. Geometric models

The first step for a computational analysis is the choice of the geometric model to use in the simulations that will accurately represent the porous medium. In this work we have chosen two different representations.

3D RANDOM PACKING The first model is a random packing of uniform spheres, which was built via rigid-body simulations using the software `Blender`. This method was chosen amongst other possible alternativs (e.g. DEM codes) for its low computational cost, ease of use and accessibility (it being a free and open source code). Its effectivess in the creation of realistic packings used in the context of simulation of chemical reactors was explored and proved in the literature and previous works [42, 43]. The code performs a rigid-body simulation by solving Newton's equations of motion for a system of N spherical bodies [4] and the grains are considered hard spheres when it comes to calculating the interactions between them. This means that there are only instantaneous interactions and any compenetration is impossible. A number of other features of the solid grains has to be specified in the rigid body simulation, among which the grains restitution coefficient and their attrition coefficient. These two features are very important for the resulting packing structure, having a noticeable effect on porosity and the presence (or absence thereof) of large-scale heterogeneities of the packing. More details on the choice of these and other simulation parameters can be found in a previous work [42], along with their validation with available experimental data.

With this setup, the loading of a cylindrical container was simulated, above which the solid grains are initially placed. Then, an uniform force representing gravity is applied to all the particles, forcing them to fall inside the container. The final state of the packing simulation is obtained when all particle motion stops, which means a balance is reached between the different forces acting upon them (i.e. gravity and interaction forces). The details of the container, the number of particles used in the simulation, and their diameter are found in Tab. 1. The choice of both the number of grains used and the size of the cylindrical container were dependent on the necessity of creating a *Representative Elementary Volume* (REV) to use in the CFD simulations. The following sections, before the presentation of the actual simulation results regarding deposition efficiency, will show the procedure for the extraction and validation of the size of this representative volume. Figure 1 shows a typical packing obtained with a `Blender`

[4] While in this work we have chosen for simplicity to study the case of a packing of uniform spheres, it is possible to create packings of arbitrary shapes with `Blender`, as shown in [42].

simulation as described here, and the resulting computational domain that can be extracted from it.

Container diameter (mm)	2.15
Container heigth (mm)	1.86
Number of solid grains	7800
Diamter of solid grains (μ m)	100

Table 1: Numerical details of the packing created with `Blender`.

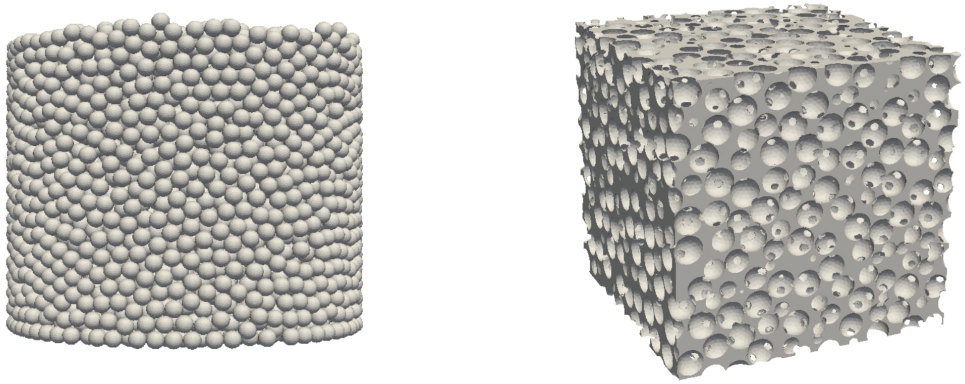

Figure 1: Computer-generated geometric model for the random spheres packing. On the left, the original cylindrical packing of uniform spheres created with `Blender`. On the right, the extracted computational volume used in the simulations.

3D ARRANGED PERIODIC MODEL The second model considered is also three-dimensional, but a much simpler structure was generated, without recurring to rigid-body simulations. An arranged packing of spheres was built, with their spatial positioning following a face-centered cubic (FCC) lattice (referring to the crystal systems naming nomenclature). This results in a regular and periodic geometry characterized by the presence of several planes of symmetry which can be used to reduce the domain to its fundamental repeating unit and thus dramatically reduce the computational cost: this is especially important when dealing with a more complicated physical and modelling setup than the one required for the simple solution of the advection-diffusion equation, as is the case of the solution of the momentum transport equations used for the simulation of transport of polydisperse particles, treated in the last part of the current work.

While these arranged packings are evidently not realistic for the representation of randomly packed media, they were successfully employed in the study of particle dispersion, and their behaviour has been shown to be equivalent to that of packed systems exhibiting Fickian dispersion [44].

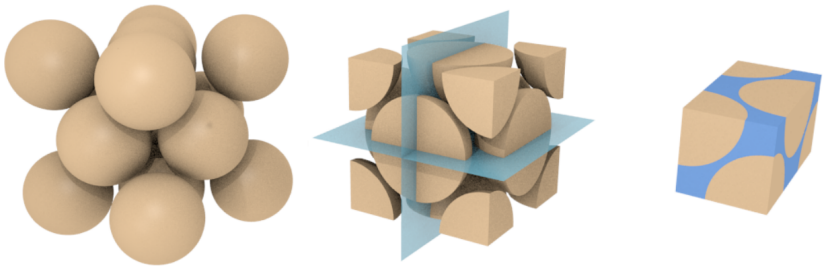

Figure 2: Representation of the face-centered cubic model. In evidence, from left to right: the original arranged structured, the three main planes of symmetry, and finally the actual reduced structure used in the simulations.

3.2. Grid convergence of the results

A crucial element in the pre-processing step of a CFD simulation is the generation of the computational mesh, and particularly the attainment of a refined enough mesh for which the results can be considered *grid independent*. This procedure has to be conducted with great care, especially in the case of three-dimensional random geometries, for which a direct control on the meshing strategy is impossible. For this reason, here we will treat these more complicated geometries, and refer the reader to other previous works [44] describing the grid convergence study for the FCC periodic arrangements. The grids, as mentioned, were created with the open-source code `OpenFOAM`, using as a starting geometry a cubic cut extracted from the geometrical center of the packing generated with `Blender`, akin to what is shown in Fig. 1 (right). The meshing process was constituted of two steps performed by the use of two `OpenFOAM` meshing utilities: first `blockMesh` was used to create a (stair-stepped) structured cartesian mesh in the inter-granular voids, which was then converted to a body-fitted mesh representing the actual shape of the spherical grains by using `snappyHexMesh`. To obtain the most beneficial trade-off between a smaller mesh (i.e. less computationally expensive) and the reduction of simulation errors due to the spatial discretization, a number of different meshes with increasing cell number and differing in meshing strategy were created and tested: the details of these different meshes are found in Tab. 2. The refinement operation was conducted both by using a smaller cell size for the starting structured mesh (resulting in an uniform refiment), and also refining the cells adjacent to the solid grains. This was done via a cell splitting operation, transforming one boundary cell into an octree partition. The rationale for a refinement on the surface is simply to expend the most number of cells in the domain zones where it is possible to expect larger gradients of the properties under study (e.g.: fluid velocity, particle concentration).

While the study of grid convergence relative to fluid flow have already been performed in previous works [42], the accuracy of these setups with respect to the simulation of particle deposition in random packings still has to be as-

Case	Cells per diameter	Surface refinement
I	16	0
II	18	0
III	16	1
IV	18	1
V	20	1
VI	22	1
VII	24	1
VIII	26	1
IX	30	1

Table 2: Different grids examined in the grid convergence study. Cell density expressed as the ratio between the spherical grain diameter and the cell linear size, with varying levels of surface refinement (e.g.: with one surface refinement corresponding to one single operation of cell splitting.)

certained. To this end, simulations of fluid flow and particle transport and deposition (solving the advection-diffusion equation) were performed on each of the grids in Tab. 2, on a cubic domain of side equal to $700\mu m$, constituted of approximately 350 grains. The operating conditions used to perform this grid indepence analysis were $\mathrm{Re} = 2.5 \cdot 10^{-4}$ and $\mathrm{Pe} = 175$, corresponding to a molecular diffusion coefficient $\mathcal{D} = 1.43 \cdot 10^{-12}$ [5]. In each of these cases, the Brownian deposition efficiency η_B was calculated, and the results are shown in Fig.3. As it can be seen, with increasing cell numbers the deposition efficiency for the Brownian mechanism present an asymptote starting from the fifth datapoint (mesh V), representing a mesh characterized by a density equal to 20 cells per diameter, with one subsequent surface refinement. As shown in the work mentioned previously [42] and [45], this mesh is also sufficient to reach grid convergence with respect to fluid flow, while it has to be noted that the accuracy may decrease with increasing Péclet number (i.e.: increasing concentration gradients). This meshing strategy was then employed in all cases, resulting in a mesh of 19 million cells for a sample containing approximately 1000 grains. The difference in mesh cell number (and size sample) with respect to the ones just explored lies in the fact that while the size of this sample is sufficient to qualitatively describe a uniform random packing in the terms of the identification of the correct meshing strategy to use, it still does not constitute a REV, as it will be seen in the next section.

3.3. Extraction of the REV

As mentioned, after the identification of a suitable meshing strategy, we have identified the representative elementary volume for the system, from which

[5] For more details about the computational setup and boundary conditions, refer to the later section about the study of deposition efficiency in the monodisperse case, for they are common throughout this section and the following related to the identification of the REV.

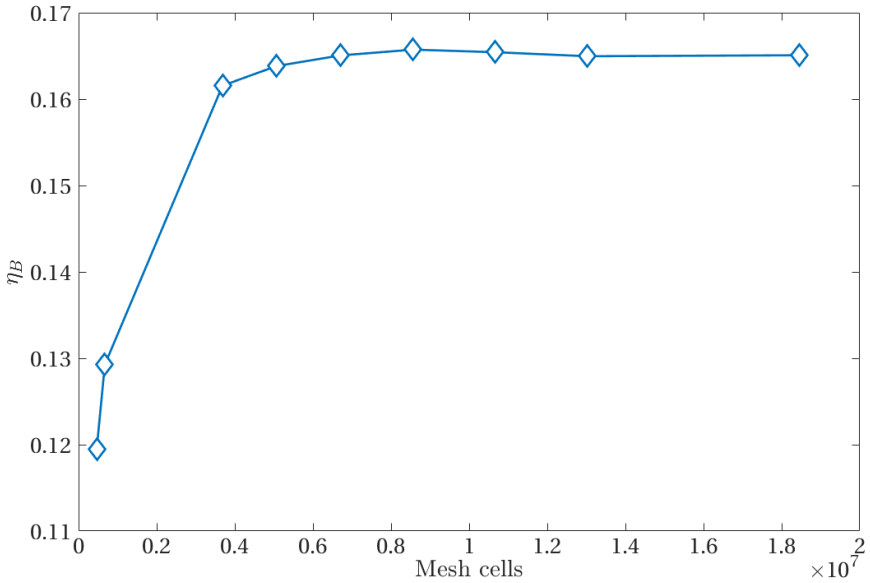

Figure 3: Brownian deposition efficiency with increasing mesh refinement, Pe=175.

appropriate results of deposition efficiency can be extracted. The concept of a representative elementary volume is statistical in nature, and the process for its identification is connected to the individuation of the minimum volume (i.e.: sample size) with which it is possible to accurately represent the evolution of a physical phenomenon, or its physical structure.

For this purpose, we performed simulations of particle transport and Brownian deposition on a series of computational domains, with the same operating conditions throughout, Re = 10^{-2} and Pe = 200. Each of these domains is a cubic cut as shown in Fig. 1, with increasing size: the smallest domain contains approximately 200 grains, while the bigger one contains 1200 grains. Moreover, to also take into account the randomness of the structure of the packings, we repeated this process three times, each with a different geometric realization (i.e.: a different packing created with `Blender`). Figure 4 shows the resulting deposition efficiency versus increasing sample size for the three realizations: the results show that in the case of particle deposition, a suitable REV is given by a sample containing about 1000 grains, after which the value of deposition efficiency does not change with marginal increases in sample size. The three different packings show very similar trends of deposition efficiency with respect to sample size: the coefficient of variation of the three data-points is about 2%.

Finally, the size of REV obtained for the modelling of particle deposition is also larger than needed and thus appropriate for the description of fluid flow and the geometric structure of the medium (expressed via its porosity). While

we don't show the graphs here, for brevity, the same analysis was performed as the one just shown, resulting in even smaller REV sizes, of about 600 grains. On the other hand, the analysis regarding the mechanism of deposition by sedimentation is more complex, especially with respect to the possibility of different relative orientation of the gravitational acceleration and the mean direction of fluid flow, and will be treated in later studies.

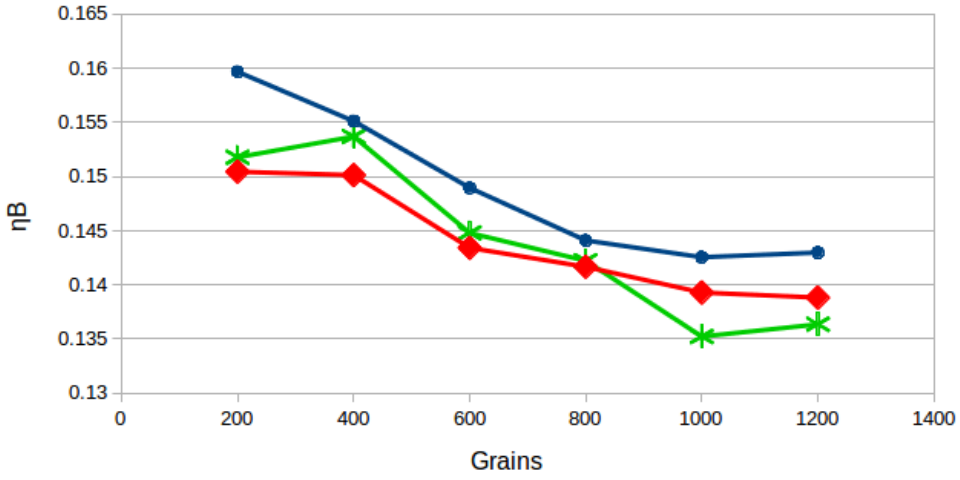

Figure 4: Brownian deposition efficiency with increasing domain size (in terms of number of grains), for three different random packings (different symbols/colors).

3.4. Monodisperse case: Brownian and sedimentation efficiency

All simulations of fluid flow and particle deposition were performed with the open-source code `OpenFOAM`, which is also used for the pre-processing (i.e. meshing) step. Both systems with only Brownian deposition and systems with Brownian and sedimentation deposition were considered: in both cases, three different geometric realizations of a randomly packed porous medium were studied. In the first case, the domain considered was a cubic cut with a side of 1 mm in all three dimensions, containing approximately 1000 grains, each with diameter equal to 100 μm, with an average porosity $\varepsilon = 0.352$: this choice came from the REV analysis just presented. When dealing with the more complex case of sedimentation, considered the need of performing multiple simulations taking into account the different relative directions of gravity with respect to the fluid direction, a smaller domain (from the same original `Blender` packings) containing approximately 350 grains was used. First, fluid flow simulations were performed in these domains, by solving Eq. 1 by setting a pressure drop between two opposite side of the cubic domain, driving fluid flow in the direction orthogonal to the two faces. The remaining faces were set as symmetry boundaries, which means setting a null gradient of the considered properties and effectively

making the boundaries impermeable to diffusive and advective flow. We consider the fluid to be water, Newtonian and incompressible and in isotherm conditions, with density $\rho = 997.78$ Kg·m^{-3}, and viscosity $\mu = 0.001003$Kg·m^{-1}s^{-1}. The resulting fluid flow field was used in the simulations of particle transport working, as mentioned, under the assumption of one-way coupling between the particles and the fluid motion. The important difference discerning whether particle sedimentation has to be ignored or considered in the particle deposition simulations, is that in the latter case the particle terminal sedimentation velocity vector (whose orientation depends on the chosen gravity direction) is added uniformly to the obtained fluid flow field.

Then, simulations solving Eq. 2 at the steady state are performed. Particles are injected in the system by means of setting a unitary value of normalized particle concentration in the inlet face. As it was done in previous and other works [28, 35] to represent the perfect sink boundary condition, the value of particle concentration on the surface of solid grains was set equal to zero while, as in the case of fluid flow, the remaining lateral faces were set up as symmetrical boundaries.

Reynolds number	Particle diameter (nm)	Péclet number
10^{-4}	96	22
10^{-4}	257	59
10^{-3}	69	158
10^{-3}	185	425
10^{-2}	50	1140
10^{-2}	133	3057
10^{-1}	36	8200
10^{-1}	96	22000

Table 3: Reynolds numbers and particle diameters for each Brownian deposition simulation, and the resulting Péclet number.

Table 3 shows the operating conditions of the case of Brownian deposition without sedimentation, while a snapshot of the results can be found in Fig. 5, showing contour plots of particle concentration in in the middle section of one of the three geometric realization in the case of Brownian deposition (without sedimentation), for increasing particle size (and thus, increasing Péclet number). As expected, particle deposition is increased for smaller Péclet numbers, which is due to the concurrent effects of particle size and fluid velocity. Particles with smaller diameter are characterized by a greater Brownian mobility and thus an increased transport from the bulk of the fluid to the surface of the porous medium, where they are removed by deposition; lower fluid velocities result in higher time spent by the particles in the domain before their escape, and thus higher probability of being transported to the grains surface by molecular diffusion. The final point is to calculate the Brownian deposition efficiency from the values of obtained values of particle concentration via Eq. 9 over all the range of Péclet numbers considered: the results are shown in Fig. 6.

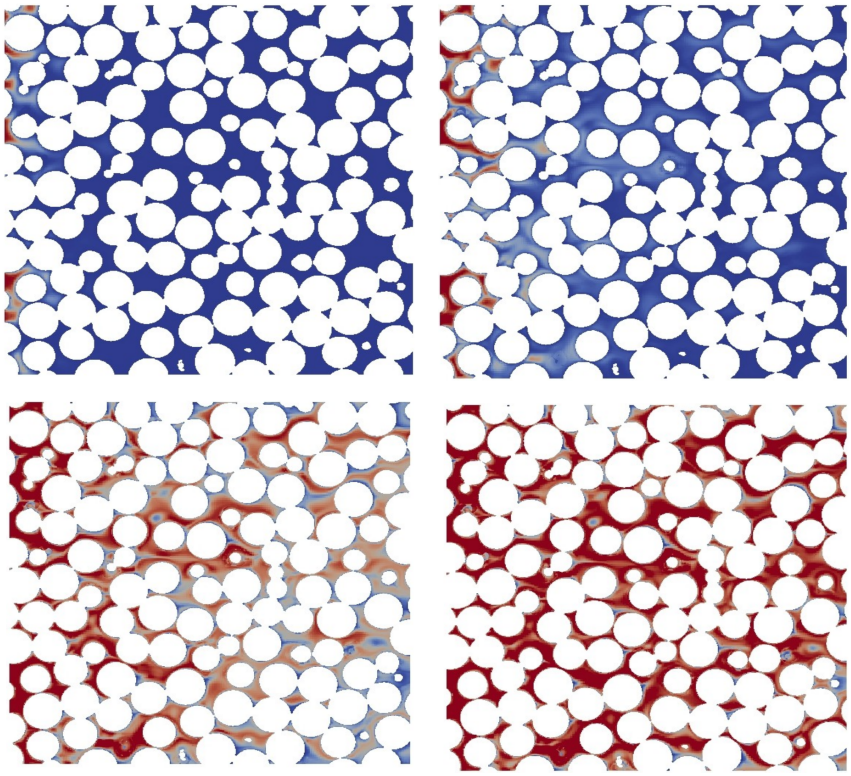

Figure 5: Contour plots of particle concentration in the a median section (parallel to fluid flow) inthe case of Brownian deposition for the same geometry and different particle diameters. From top to bottom and from left to right, Pe = 22, Pe = 158, Pe = 3057,Pe = 22000.

The graph shows how the results follow the trend of the theoretical predictions, with a marked separation for low Pe. This is manly due to the fact that the original work by Levich [28] does not take into account the contribution of diffusive flux in the balance of mass entering the system, which is especially relevant for lower Pe. Employing the classical laws directly in these regimes may lead to unphysical results, e.g. values of efficiency η greater than one: this has been evidenced in other works [46, 47, 48]. For this reason, in the context of this work where the purpose is to compare the simulations results to the theoretical law in their range of applicability, we will exclude the results relative to the lowest Péclet number (Pe=22). The remaining data can be described by a

constituive equation in the same form of 10:

$$\eta_B = CAs^{1/3}\mathrm{Pe}^{\alpha} \ , \tag{12}$$

which results, after operating a regression on the average of the values of the three geometric realizations, in:

$$\eta_B = 0.83As^{1/3}\mathrm{Pe}^{0.57} \tag{13}$$

While the exponent α shows a minor variation from the value in the theoretical law, the pre-exponential coefficient C is instead markedly different. This can be explained by deviation from the ideal conditions of the systems taken here under consideration, which are meant to represent realistic packings: in this light, it is clear how the random arrangement of grains of these packings breaks the ideality of Happel's model, modifying the interaction of the grains on each other's concentration boundary layers in non-trivial ways.

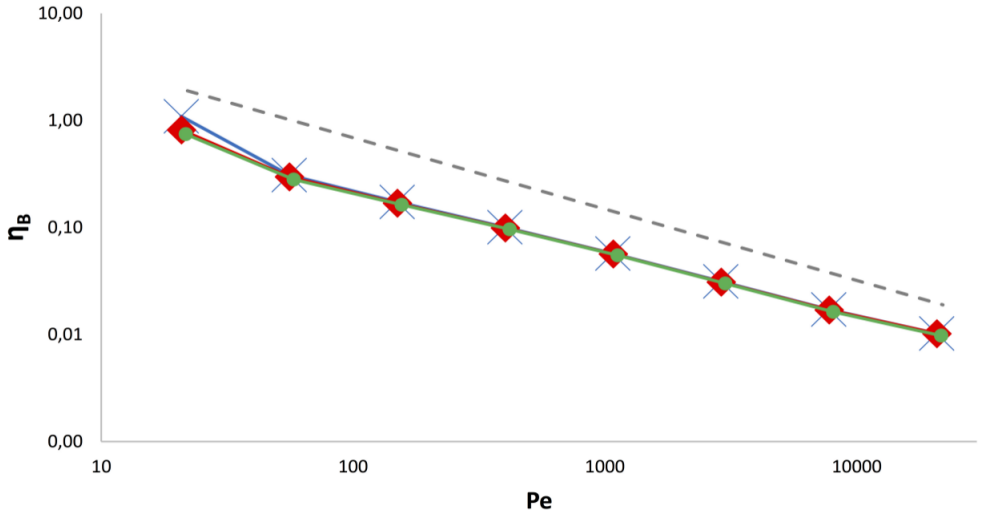

Figure 6: Brownian deposition efficiency with varying Péclet number, for three different random packings (different symbols/colors), compared with theoretical Happel's law (dashed grey line). All datapoints are normalized by the respective porosity-dependent value $As^{1/3}$.

Then, the effect of particle sedimentation on deposition efficiency was considered. As mentioned a new simulation campaign was performed, where the particle terminal sedimentation velocity was added to the obtained fluid flow field, to replicate the effect of the deviation of velocity of the particles subjected to gravitational acceleration, which in these first cases was considered to be orthogonal to the fluid direction. As before, three differerent geometric realizations of a random packing were used. The operating conditions, spanning a wide range of gravity numbers N_G, are reported in Tab. 4, and for the purposes of calculating the settling velocity with Eq. 3, $\rho_s = 7860$ kg m^{-3}

(i.e.: iron). Figure 7 shows the effect of the additional transport mechanism, markedly increasing particle deposition and skewing the spatial distribution of concentration towards the direction of gravity.

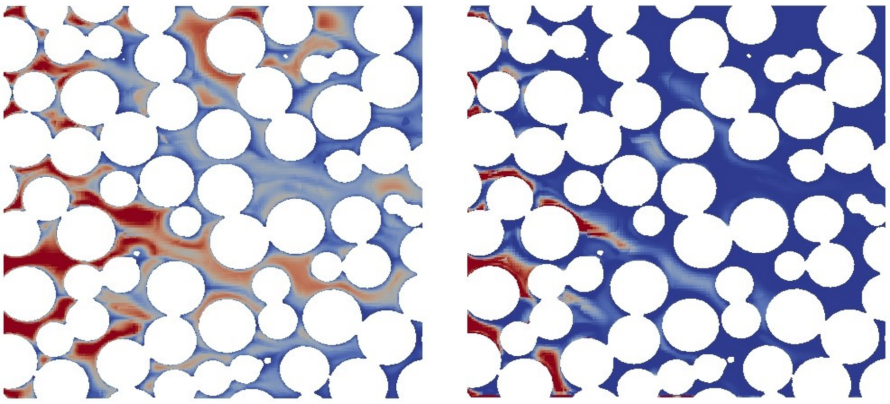

Figure 7: Comparison between contour plots of particle concentration in a median section of the same geometric domain, for the same Péclet number Pe = 588, showing the effect of particle sedimentation (right) with respect to the only Brownian deposition, without gravitational effects (left). The direction of gravity here (from top to bottom) is orthogonal to fluid flow (left to right).

Reynolds number	Particle diameter (nm)	Settling velocity ($\mathrm{m{\cdot}s^{-1}}$)	N_G	Péclet number
$2.85 \cdot 10^{-4}$	897	$2.85 \cdot 10^{-6}$	0.35	588
$3.33 \cdot 10^{-4}$	897	$2.85 \cdot 10^{-6}$	0.3	686
$4 \cdot 10^{-4}$	897	$2.85 \cdot 10^{-6}$	0.25	823
$5 \cdot 10^{-4}$	897	$2.85 \cdot 10^{-6}$	0.2	1026
$6.7 \cdot 10^{-4}$	897	$2.85 \cdot 10^{-6}$	0.15	1374
10^{-3}	897	$2.85 \cdot 10^{-6}$	0.1	2060
10^{-4}	634	$1.43 \cdot 10^{-6}$	0.05	1456

Table 4: Reynolds numbers and particle diameters for each Brownian deposition simulation with sedimentation, and the resulting Péclet number and gravity number N_G.

Considering that $\eta_{TOT} = \eta_B + \eta_G$ [49], the results of sedimentation deposition efficiency η_G can be obtained by subtraction, performing two simulations on the same system respectively with or without the addition of the particle sedimentation velocity and separating the two different contributions. These results are shown in Fig. 8 (top), where the trends for each of the three different realizations are:

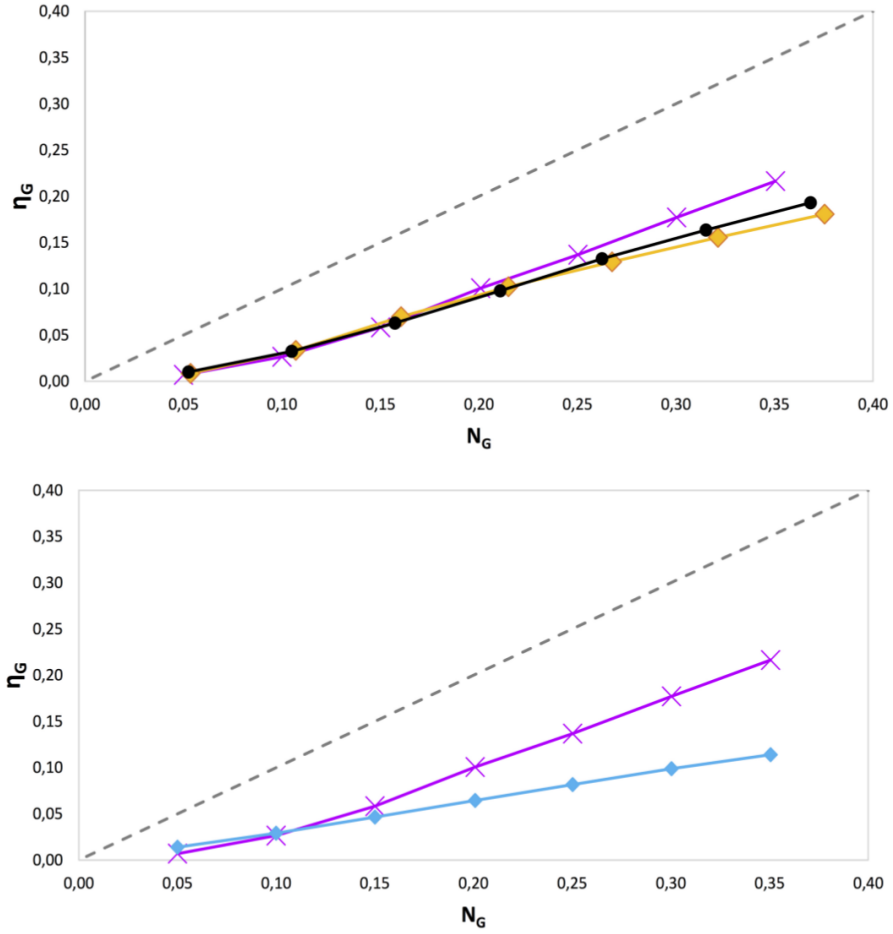

Figure 8: Sedimentation efficiency η_G for different values of gravity number N_G. On the top, results for three different random packings (different symbols/colors). On the bottom, results for the case of gravity acting in a direction parallel to fluid flow (purple line) and orthogonal to fluid flow (blue line). In both figures, the theoretical law is reported for comparison (dashed grey line).

$$\begin{aligned} \eta_G &= 0.72 N_G - 0.04 \\ \eta_G &= 0.55 N_G - 0.02 \\ \eta_G &= 0.60 N_G - 0.03 \, . \end{aligned} \tag{14}$$

These constitutive equations differ from theoretical expectation of $\eta_G = N_G$, again this shows the inadequacy of Yao's simplified model to describe randomly arranged systems. It can also be noticed that the trends of each geometry

diverge for increasing N_G: this is instead most probably due to the fact that the smaller computational domains here considered do not represent a REV for this system, and thus evidences a point which will need further investigation, as was done in the case of Brownian deposition. Together with this, another point worth exploring is the effect that grain diameter could have on sedimentation efficiency, which is another parameter missing in the theoretical description of the problem.

Lastly, for one of the geometric models used, two different simulations at the same operating conditions (i.e.: Reynolds and Péclet number) were performed, examining the different behaviour in the case where the direction of gravitational acceleration is respectively orthogonal or parallel to the mean fluid flow direction. The results of sedimentation efficiency for the two cases versus gravity number are shown in Fig. 8 (bottom), and the two trend lines are described by the equations:

$$\begin{aligned} \eta_G &= 0.72 N_G - 0.04 \\ \eta_G &= 0.34 N_G - 0.04 \,, \end{aligned} \tag{15}$$

both quite different from the theoretical prediction. The difference between the two cases can be ascribed to the lower particles residence time in the case of parallel gravity[6], leading to a decrease in the time available to the particles to reach the grains surface and hence a depressed deposition.

3.5. Polydisperse case: effects on size evolution and efficiency

In the second part of this work, we explore the effect of considering the particles as a polydisperse population, instead of a concentration of particles with uniform diameter; only the Brownian mechanism of deposition will be explored here. For this more complex case instead of the three-dimensional random packings obtained with `Blender`, the simplified and periodic arranged FCC geometry described in the earlier section was used; the diameter of the grains in the domain considered is equal to $D_g = 200$ μm, with porosity $\varepsilon = 0.4$. The setup of the boundary conditions is the same as the previous case, with fluid flow simulations set up with a pressure drop between the inlet and outlet faces of the domain (with added condition of periodicity of the velocity field on these two faces), with symmetry conditions on the remaining boundaries. To investigate particle deposition the classic advection-diffusion equation is not sufficient anymore, but we solved the equation of transport of the moments of the particle distribution (Eq. 5), so instead of setting a inlet boundary condition of constant unitary concentration, a constant particle distribution was set[7].

[6] This is because, in this case, the average fluid velocity magnitude after adding the particle settling velocity to the advective term of the transport equation is higher with respect to the orthogonal case.

[7] To represent the perfect-sink boundary condition, the moments of the distribution were set to a very small fraction (i.e. 1% of the inlet value, as using values equal to zero like

Figure 9 shows contour plots of the first four transported moments in the FCC domain.

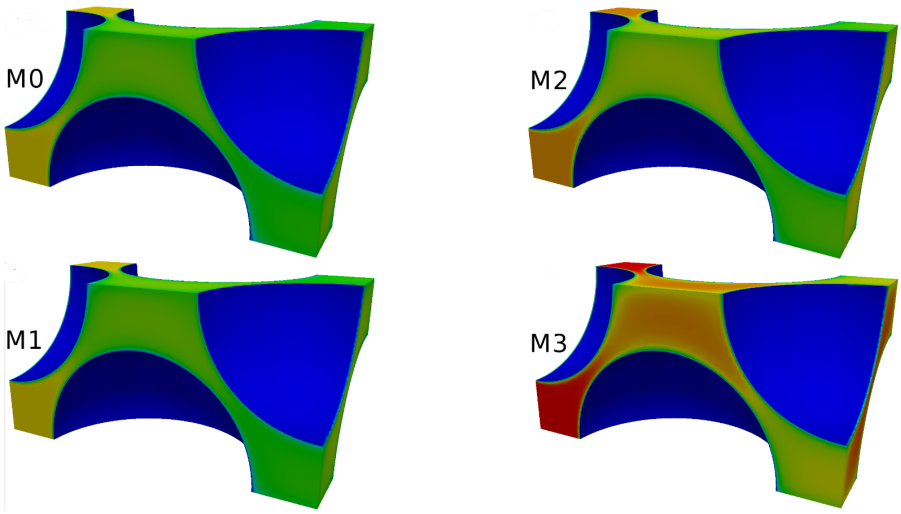

Figure 9: Contour plot of the transported moments in the case of polydisperse particle deposition in the arranged face-centered domain, values visible on the external boundaries. From left to top and top to bottom, moments from m_0 to m_3.

Specifically, we considered two cases of log-normal distributions, both with average diameter $\mu = 300$ nm, and standard deviation σ=0.3μ and σ=0.6μ, respectively. First, we performed a number of simulations exploring a range of different average fluid velocities, with Reynolds numbers from $\mathrm{Re} = 3 \cdot 10^{-3}$ to $\mathrm{Re} = 3$. From these we calculated the variation in particle Sauter diameter between the inlet and the outlet, for all fluid velocities and for the two different values of distribution standard deviation. The results are shown in Fig. 10, and it is possible to see how this ratio will always increase. This is to be expected: as already pointed out earlier, the deposition efficiency will be enhanced for lower fluid superficial velocities, as the particles residence time will be higher resulting in more time available for the diffusion mechanism to tranport them from the bulk of the fluid to the surface of the grains. Since we are considering Brownian deposition only, the smaller particles will be preferentially removed, changing the mean size at the outlet of the system to larger values, as it can be seen in Fig. 10, which shows an increment of several percentage points for the lower fluid velocities. Keeping in mind that these simulations were performed on a very small section of the periodic arrangement equal to approximately 1.2 equivalent grain diameters (refer to the rightmost image in Fig. 2 for a visualization), this means that this effect of variation on mean particle size can not be ignored when

it was done in the previous monodisperse case would cause stability issues in the moment reconstruction algorithm.

upscaling the results to the macroscopic scale, since it will have a very noticeable effect on the macroscopic transport characteristics of the particle population.

Lastly, to provide for an updated macroscopic interpretation of deposition efficiency in this case of polydisperse particles, simulations at different Péclet numbers were performed and the value of η_B calculated, similarly to the case of monodisperse particles. The results can be seen in Fig. 11, which shows a comparison between values of deposition efficiency for the theoretical (Happel's) law and both monodisperse and polydisperse cases. While in both cases the trend of the simulations results follow the theoretical law, insofar as the deposition efficiency decreases for an increasing particle size (i.e. increasing Péclet number), the polydisperse case shows a more marked departure from the theoretical predictions, and potentially reveals a different type of power law dependence for the deposition efficiency. Moreover, as it has been mentioned, it has to be noted that while Fig. 11 shows different symbols for the polydisperse case (for ease of comparison to the simple monodisperse case), the results were obtained from a single CFD simulation, which while involving the solution of multiple equations (as opposed to the single advection-diffusion when considering a constant particle size) for the transport of the distribution moments, means that great computational savings are obtained by removing the need for a potentially very large simulation campaign due to the need of considering a wide set of monodisperse cases.

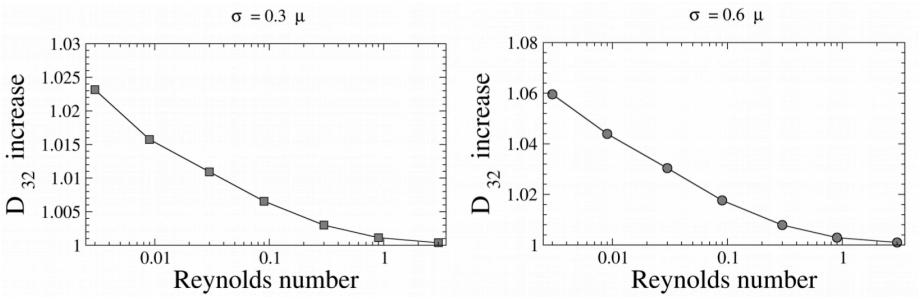

Figure 10: Evolution of the Sauter diameter with increasing Reynolds number in the face-centered simplified geometries at two different standard deviations of the particle distribution (σ=0.3μ on the left and σ=0.6μ on the right).

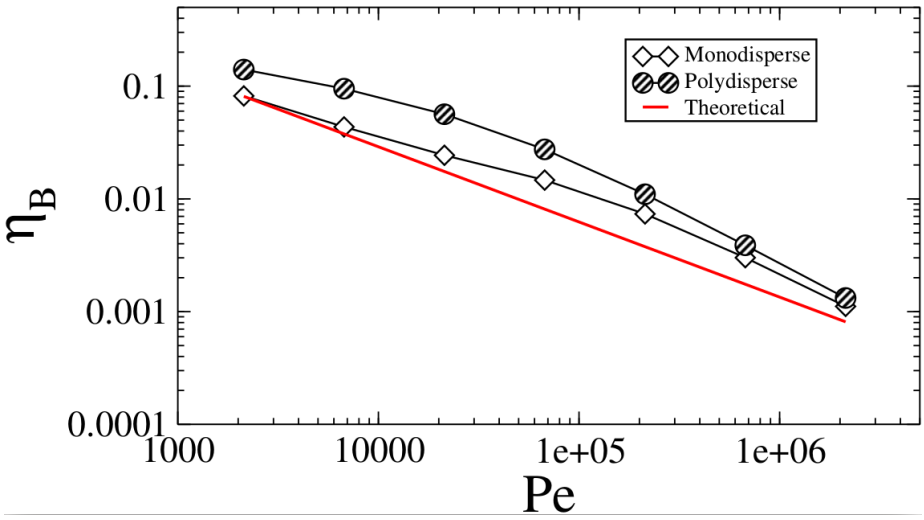

Figure 11: Deposition efficiency versus Péclet number: comparison between the theoretical law (red continuous line), monodisperse (white diamonds) and polydisperse (filled circles) systems. The standard deviation of the polydisperse population distribution at the inlet is $\sigma = 0.3\mu$.

4. Conclusions

In this work we presented a completely *in-silico* framework for the investigation of particle transport and deposition in filtration and catalytic processes. The use of the presented methodology for the creation of random packings offers two distinct advantages. First, the computer generation of realistic models of packed beds with the desired features provides for a sizeable saving with respect to the alternative of extracting the geometric structure via more expensive experimental techniques (SEM, μ-CT, et c.) Secondly, it closes one of the most glaring gaps in the theoretical description of particle deposition in the classical filtration theory, which is based on very simplified models of arranged spherical collectors. In the second part we present the main modelling advance of this work, which is the description of the polidispersity of the particle population, which was done here via the solution of the population balance equation, solved by the quadrature method of moments. The results from these simulations also show a marked difference with respect to the theoretical predictions and evidence the pitfalls of the simplified description valid for monodisperse populations, evidencing how the proposed model can greatly improve the description of particle transport and deposition in real filtration and catalytic processes.

A number of possible improvements on this work are possible. First, a more accurate representation of the porous medium will be very useful, in terms both of introducing the polidispersity of the solid grains constituting the packing, and considering non-spherical shapes. Then, even more crucially, the present results on the modelling of filtration of polydisperse transported populations will have to be expanded to include the remaining deposition mechanisms, namely interception and gravity; the inclusion of aggregation and breakage processes will also be possible in the proposed computational framework. These aspects will be studied in future works, for which the present study is meant to be the starting point.

In closing, it has to be noted that the results of the present work can be used in other fields beyond catalytic reactor engineering: in general this simulation and upscaling framework can be employed in every system characterized by a multi-scale geometric arrangement, for which it is possible to identify a separation of scales and where the phenomena at the pore-scale have an impact on the system behaviour at the macroscopic scale. By way of example the system at large scale could be, other than a catalytic reactor (structured or randomly arranged), an aquifer where studies of contaminant transport or remediation have to be carried out, or an oil reservoir suitable for EOR practices, needing precise estimations of the migration of a dispersed phase.

Acknowledgements

We acknowledge the CINECA award under the ISCRA initiative and HPC@POLITO (http://www.hpc.polito.it) for the availability of high performance computing resources and support. We also want to acknowledge the valuable contribution of Valeria Bizzarro to the present work.

References

[1] E. Cauda, D. Fino, G. Saracco, V. Specchia, Preparation and regeneration of a catalytic diesel particulate filter, Chemical Engineering Science 62 (18-20) (2007) 5182–5185.

[2] D. Fino, P. Fino, G. Saracco, V. Specchia, Innovative means for the catalytic regeneration of particulate traps for diesel exhaust cleaning, Chemical Engineering Science 58 (3-6) (2003) 951–958.

[3] S. Bensaid, D. Marchisio, D. Fino, G. Saracco, V. Specchia, Modelling of diesel particulate filtration in wall-flow traps, Chemical Engineering Journal 154 (1-3) (2009) 211–218.

[4] S. Bensaid, D. Marchisio, D. Fino, Numerical simulation of soot filtration and combustion within diesel particulate filters, Chemical Engineering Science 65 (1) (2010) 357–363.

[5] A. Lejeune, M. Rabiller-Baudry, T. Renouard, B. Balannec, Y. Liu, J. Augello, D. Wolbert, Assessment and potential of membrane cascades for organic solvent nanofiltration of hydroformylation media through a graphical representation composed of performance maps, Chemical Engineering Science 183 (2018) 240–259.

[6] R. Kolakaluri, E. Murphy, S. Subramaniam, R. Brown, R. Fox, Filtration model for polydisperse aerosols in gas-solid flow using granule-resolved direct numerical simulation, AIChE Journal 61 (11) (2015) 3594–3606.

[7] A. G. Dixon, M. Nijemeisland, Cfd as a design tool for fixed-bed reactors, Industrial & Engineering Chemistry Research 40 (23) (2001) 5246–5254.

[8] F. Augier, F. Idoux, J. Delenne, Numerical simulations of transfer and transport properties inside packed beds of spherical particles, Chemical Engineering Science 65 (3) (2010) 1055–1064.

[9] S. Tenneti, R. Garg, S. Subramaniam, Drag law for monodisperse gas–solid systems using particle-resolved direct numerical simulation of flow past fixed assemblies of spheres, International journal of multiphase flow 37 (9) (2011) 1072–1092.

[10] W. Regulski, J. Szumbarski, K. Gumowski, J. Skibiński, M. Wichrowski, T. Wejrzanowski, et al., Pressure drop in flow across ceramic foamsa numerical and experimental study, Chemical Engineering Science 137 (2015) 320–337.

[11] G. I. Garrido, F. Patcas, S. Lang, B. Kraushaar-Czarnetzki, Mass transfer and pressure drop in ceramic foams: a description for different pore sizes and porosities, Chemical Engineering Science 63 (21) (2008) 5202–5217.

[12] M. Lacroix, P. Nguyen, D. Schweich, C. P. Huu, S. Savin-Poncet, D. Edouard, Pressure drop measurements and modeling on sic foams, Chemical Engineering Science 62 (12) (2007) 3259–3267.

[13] J. von Rickenbach, F. Lucci, P. D. Eggenschwiler, D. Poulikakos, Pore scale modeling of cold-start emissions in foam based catalytic reactors, Chemical Engineering Science 138 (2015) 446–456.

[14] E. Crevacore, G. Boccardo, D. Marchisio, R. Sethi, Microscale colloidal transport simulations for groundwater remediation, Chemical Engineering Transactions 47 (2016) 271–276. doi:10.3303/CET1647046.

[15] D. Jain, Y. M. Lau, J. Kuipers, N. G. Deen, Discrete bubble modeling for a micro-structured bubble column, Chemical Engineering Science 100 (2013) 496–505.

[16] D. Jain, J. Kuipers, N. G. Deen, Numerical modeling of carbon dioxide chemisorption in sodium hydroxide solution in a micro-structured bubble column, Chemical Engineering Science 137 (2015) 685–696.

[17] Q. Segers, J. Kuipers, N. Deen, Immersed boundary method applied to single phase flow past crossing cylinders, Chemical Engineering Science 100 (2013) 33–38.

[18] C. Yuan, F. Laurent, R. Fox, An extended quadrature method of moments for population balance equations, Journal of Aerosol Science 51 (2012) 1–23.

[19] E. Madadi-Kandjani, A. Passalacqua, An extended quadrature-based moment method with log-normal kernel density functions, Chemical Engineering Science 131 (2015) 323 – 339. doi:https://doi.org/10.1016/j.ces.2015.04.005.
URL http://www.sciencedirect.com/science/article/pii/S0009250915002559

[20] D. L. Marchisio, R. O. Fox, Computational models for polydisperse particulate and multiphase systems, Cambridge University Press, 2013.

[21] F. Laurent, Numerical analysis of eulerian multi-fluid models in the context of kinetic formulations for dilute evaporating sprays, ESAIM: Mathematical Modelling and Numerical Analysis 40 (3) (2006) 431–468.

[22] M. Massot, F. Laurent, D. Kah, S. De Chaisemartin, A robust moment method for evaluation of the disappearance rate of evaporating sprays, SIAM Journal on Applied Mathematics 70 (8) (2010) 3203–3234.

[23] M. Elimelech, J. Gregory, X. Jia, R. A. Williams, Particle Deposition and Aggregation, Butterworth-Heinemann, Woburn (MA), 1995.

[24] C. Tien, Granular Filtration of Aerosols and Hydrosols: Butterworths Series in Chemical Engineering, Butterworth-Heinemann, 2013.

[25] R. Rajagopalan, C. Tien, Trajectory analysis of deep-bed filtration with the sphere-in-cell porous media model, AIChE Journal 22 (3) (1976) 523–533.

[26] A. C. Payatakes, C. Tien, R. M. Turian, A new model for granular porous media: Part i. model formulation, AIChE Journal 19 (1) (1973) 58–67. doi:10.1002/aic.690190110.
URL http://dx.doi.org/10.1002/aic.690190110

[27] B. Logan, D. Jewett, R. Arnold, E. Bouwer, C. O'Melia, Clarification of clean-bed filtration models, Journal of Environmental Engineering 121 (12) (1995) 869–873.

[28] V. G. Levich, Physicochemical Hydrodynamics, Prentice-Hall, Englewood Cliffs, NJ, USA, 1962.

[29] W. P. Johnson, M. Hilpert, Upscaling colloid transport and retention under unfavorable conditions: Linking mass transfer to pore and grain topology, Water Resources Research 49 (9) (2013) 5328–5341.

[30] F. Messina, T. Tosco, R. Sethi, On the failure of upscaling the single-collector efficiency to the transport of colloids in an array of collectors, Water Resources Research 52 (7) (2016) 5492–5505.

[31] G. Boccardo, E. Crevacore, R. Sethi, M. Icardi, A robust upscaling of the effective particle deposition rate in porous media, Journal of contaminant hydrology.

[32] J. Happel, Viscous flow in multiparticle systems: Slow motion of fluids relative to beds of spherical particles, AIChE Journal 4 (2) (1958) 197–201.

[33] K. M. Yao, Influence of suspended particle size on the transport aspect of water filtration, Ph.D. thesis, University of North Carolina (1968).

[34] K. M. Yao, M. T. Habibian, C. R. O'Melia, Water and waste water filtration. concepts and applications, Environmental Science & Technology 5 (11) (1971) 1105–1112.

[35] G. Boccardo, D. L. Marchisio, R. Sethi, Microscale simulation of particle deposition in porous media, Journal of Colloid and Interface Science 417 (0) (2014) 227 – 237.

[36] N. Tufenkji, M. Elimelech, Correlation equation for predicting single-collector efficiency in physicochemical filtration in saturated porous media, Environmental Science & Technology 38 (2) (2004) 529–536.

[37] E. Pazmino, M. H., W. Johnson, Applicability of colloid filtration theory in size-distributed, reduced porosity, granular media in the absence of energy barriers, Environmental Science and Technology 45 (2011) 10401–10407.

[38] H. Ma, M. Hradisky, W. P. Johnson, Extending applicability of correlation equations to predict colloidal retention in porous media at low fluid velocity, Environmental Science and Technology 47 (5) (2013) 2272–2278. doi:10.1021/es304753r.
URL http://pubs.acs.org/doi/abs/10.1021/es304753r

[39] M. Biggs, S. Humby, A. Buts, U. Tzn, Explicit numerical simulation of suspension flow with deposition in porous media: influence of local flow field variation on deposition processes predicted by trajectory methods, Chemical Engineering Science 58 (7) (2003) 1271 – 1288. doi:https://doi.org/10.1016/S0009-2509(02)00555-9.
URL http://www.sciencedirect.com/science/article/pii/S0009250902005559

[40] G. Mikolajczyk, L. Huang, M. Wilhelm, W. Dreher, S. Odenbach, Colloid deposition in monolithic porous media experimental investigations using x-ray computed microtomography and magnetic resonance velocimetry, Chemical Engineering Science 175 (2018) 257 – 266. doi:https://doi.org/10.1016/j.ces.2017.09.054.
URL http://www.sciencedirect.com/science/article/pii/S0009250917306097

[41] B. Ding, C. Li, Y. Wang, J. Xu, Effects of pore size distribution and coordination number on filtration coefficients for straining-dominant deep bed filtration from percolation theory with 3d networks, Chemical Engineering Science 175 (2018) 1 – 11. doi:https://doi.org/10.1016/j.ces.2017.09.033.
URL http://www.sciencedirect.com/science/article/pii/S0009250917305882

[42] G. Boccardo, F. Augier, Y. Haroun, D. Ferré, D. L. Marchisio, Validation of a novel open-source work-flow for the simulation of packed-bed reactors, Chemical Engineering Journal 279 (2015) 809 – 820. doi:http://dx.doi.org/10.1016/j.cej.2015.05.032.

[43] B. Partopour, A. G. Dixon, An integrated workflow for resolved-particle packed bed models with complex particle shapes, Powder Technology 322 (2017) 258 – 272. doi:https://doi.org/10.1016/j.powtec.2017.09.009.
URL http://www.sciencedirect.com/science/article/pii/S0032591017307398

[44] E. Crevacore, T. Tosco, R. Sethi, G. Boccardo, D. Marchisio, Recirculation zones induce non-Fickian transport in three-dimensional periodic porous

media, Physical Review E - Statistical, Nonlinear, and Soft Matter Physics 94 (5). doi:10.1103/PhysRevE.94.053118.

[45] M. Icardi, G. Boccardo, D. L. Marchisio, T. Tosco, R. Sethi, Pore-scale simulation of fluid flow and solute dispersion in three-dimensional porous media, Phys. Rev. E 90 (2014) 013032.

[46] N. K. E., G. T. R., New collector efficiency equation for colloid filtration in both natural and engineered flow conditions, Water Resources Research 47 (5). arXiv:https://agupubs.onlinelibrary.wiley.com/doi/pdf/10.1029/2010WR009587, doi:10.1029/2010WR009587.
URL https://agupubs.onlinelibrary.wiley.com/doi/abs/10.1029/2010WR009587

[47] K. E. Nelson, T. R. Ginn, T. Kamai, Comment on extending applicability of correlation equations to predict colloidal retention in porous media at low fluid velocity, Environmental Science & Technology 47 (14) (2013) 8078–8079. doi:10.1021/es401944q.

[48] F. Messina, D. L. Marchisio, R. Sethi, An extended and total flux normalized correlation equation for predicting single-collector efficiency, Journal of Colloid and Interface Science 446 (2015) 185 – 193. doi:https://doi.org/10.1016/j.jcis.2015.01.024.
URL http://www.sciencedirect.com/science/article/pii/S0021979715000594

[49] D. C. Prieve, E. Ruckenstein, Effect of london forces upon the rate of deposition of brownian particles, AIChE Journal 20 (6) (1974) 1178–1187. doi:10.1002/aic.690200618.
URL http://dx.doi.org/10.1002/aic.690200618

Appendix A. Accuracy of EQMOM reconstruction

As it has been mentioned elsewhere in the manuscript, the EQMOM was employed as a post-processing step for the reconstruction of the particle size distribution at the outlet of the domain, to calculate the particle deposition efficiency η. Several non-trivial choices have to be made to obtain a physical and realistic number density function from the available set of moments: one is the the number of nodes chosen, another is the kernel density function itself (here chosen to be a log-normal distribution due to its semi-infinite support). Also, it has to be remembered that the EQMOM reconstruction procedure will return a smooth number density function having the same set of moments as the original distribution (depending on the number of quadrature nodes used), but of which it is not guaranteed to be an exact representation. As it will be seen later in this Appendix, some cases can be identified in which the reconstructed and expected distribution differ greatly, but those are cases in which the use of EQMOM would indeed be inappropriate. Moreover, it is not possible

to know *a priori* whether the specific physical problem will result in a set of moments from which it is possible to extract a realistic (and accurate) particle size distribution. Thus, to inform a correct application of EQMOM to our system, we have conducted a preliminary campaign where we substituted our particle deposition system with zero-dimensional reduced models operating with a number of simple filtration "laws", for which the resulting outlet distribution is obtainable a priori. An inlet particle size distribution (expressed through its moments, as in our CFD simulations) was then subjected to these filtration 0D models, and the results reconstructed with the EQMOM. The resulting curve was compared to the theoretical expectation, resulting in a good guideline for the possibility of application of the methodology for various cases, and the its range of applicability in terms of relevant operating conditions. The three "toy models" are represented in Fig. A.12: in the figure, to each model two graphs are associated showing the corresponding concentration ratio (between outlet and inlet of the system) and the deposition efficiency versus the Péclet number. In the first case, the 0D model prescribes a step-function removal, where all particles with a size smaller than a certain threshold are removed: after this threshold the concentration ratio equals unity (no particles removed) and the deposition efficiency goes to zero. In the second case, a linear removal is posited. Instead of having a filtration threshold, the assumption is that particles with size tending to zero are completely removed (null concentration ratio, i.e.: no particles exiting the system), with a linear relationship for the concentration ratio holding for progressively larger particles. In this case the relationship between concentration ratio and deposition efficiency is non-trivial, and Eq. 9 was used to obtain η. The third case is the closest to the one of interest for us. The assumed filtration law is the classical colloid filtration theory: instead of assuming a certain concentration ratio (like in the linear model), we assume that the relationship between η and Péclet number follows a functional form similar to the power-law obtained by Yao (Eq. 10). This assumption is indeed verified, save for different values of the pre-exponential and exponential coefficients, as shown in the results of the present study and previous works [35].

The following figures show the results of this study. First, the original log-normal particle size distribution is shown, with the corresponding theoretical expectation of the outlet distribution; on the side the particle distribution reconstructed via the EQMOM is shown, for a qualitative comparison. The bottom part of the three figures shows a comparison between the expected concentration ratio and, more importantly, deposition efficiency and the calculated values from the reconstructed distribution. Figure A.13 shows the results for the step removal model. As it can be seen, even a qualitative comparison of the two size distribution curves shows an appreciable error in the reconstruction. This is even more evident when looking at concentration ratio and deposition efficiency results, which are marred by very strong oscillations and discrepancies, which are not solved by the use of more EQMOM nodes (i.e.: extending the sum of kernel density functions composing the reconstructed curve), but actually increased. While this is not a case of interest for a real application in fine particles filtration, this example goes to show how certain precautions have to be taken

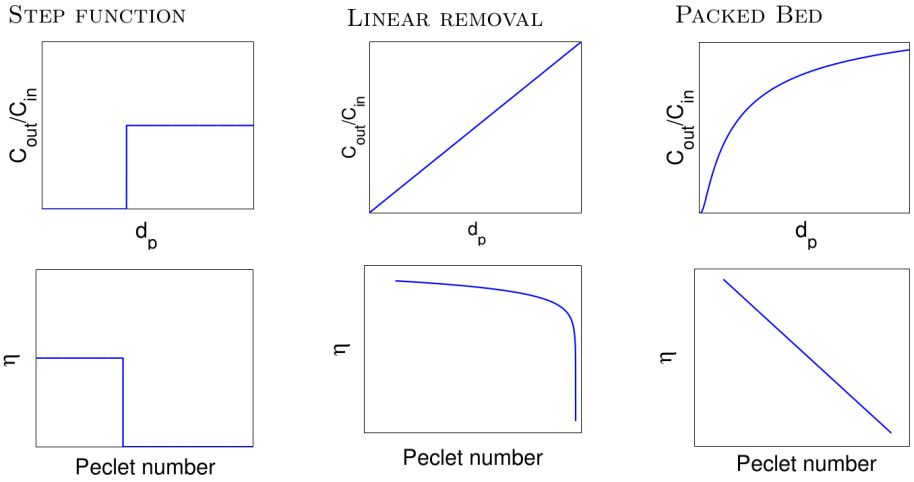

Figure A.12: Chosen 0D models, represented by the ratio of particle concentration between outlet and inlet faces $C_{\text{out}}/C_{\text{in}}$ and the corresponding deposition efficiency η versus Péclet number.

when applying this method, or even that for some cases, like the present one involving abrupt discontinuities, it is not applicable at all. As mentioned in Section 2 and earlier in this Appendix, this is not a limitation of the EQMOM. This method is based on using a sum of chosen kernel density functions to obtain a reconstruction of a smooth and continuous distribution possessing the same $2N + 1$ moments (where N is the number of quadrature nodes used) of the original density functions, which is not strictly guaranteed to conserve the original distribution shape. This is certainly true in this present case, where a clear discontinuity is present, which is obviously impossible to obtain via a sum of continuous functions. The second example of linear filtration, with data shown in Fig. A.14, paints a much brighter picture, with EQMOM being able to perfectly reconstruct a particle size distribution curve which was subjected to a system characterized by this filtration law. In this case the use of more (or less) nodes resulted in only marginal increases (or decreases) in accuracy, proving the method to be very robust. The last case, which is the one representing the actual system of interest in this work, is described in Fig. A.15. Even in this case a qualitative comparison of the expected and obtained number density functions shows a very good agreement, and resulting concentration ratio match the expected value perfectly. The interesting point comes from the observation of the last figure showing the calculated line of deposition efficiency versus Péclet number. Here it can be seen that for a wide range of Pe the results follow the power-law behaviour expected from the classical law: this is instead lost when looking at the lower and upper limit of the curve. There the calculated values deviates from the expectation, and display zones where the applicability of EQMOM breaks down. It has to be noted that these zones correspond to the tails of the distribution, corresponding to very small integral values of the density

function ($\ll 1\%$). Thus, the result of this analysis is that in the case of filtration of fine particles in packed beds, the EQMOM is a provably valid method for analysing particle deposition by analysing the outlet particle distribution curve; the caveat is that special care has to be taken when interpreting results concerning the extreme bounds of the distribution, or restrict the analysis to the part of the distribution (which is still a fraction close to 100% of the integral number of particles) where the method returns accurate results.

This is what has been done in the analysis of the very last results of this work shown in Fig. 11, where the deposition efficiency curve shown is obtained by previously "cutting" the extreme limits of the curve. As an important side note, these bounds of applicability are of course not absolute in terms of Péclet number but relative to the operating conditions, which are different between these test models and the actual simulations analyzed in this work: in other words, it is the distribution tails for which it is necessary to take care, whichever Pe they may correspond to.

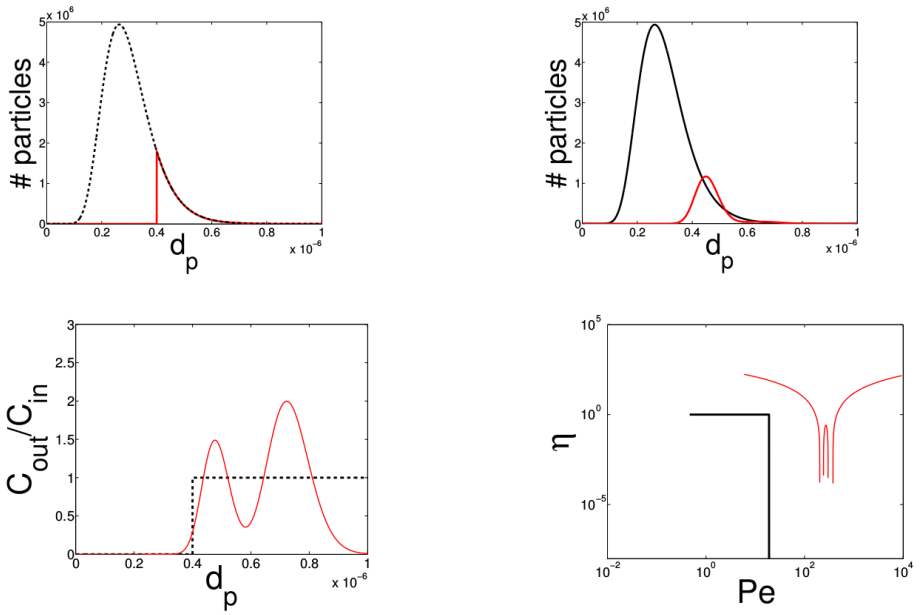

Figure A.13: Application of EQMOM (2 nodes) in the case of "step" removal. On the top left the inlet distribution (dashed black line) and the theoretical expected distribution at the outlet (continuous red line). On the top right, the resulting EQMOM reconstructed curve (continuous red line). On the bottom, the theoretical expected results (black lines) and reconstructed results (red lines) calculating inlet-outlet concentration ratio (left) and deposition efficiency (right).

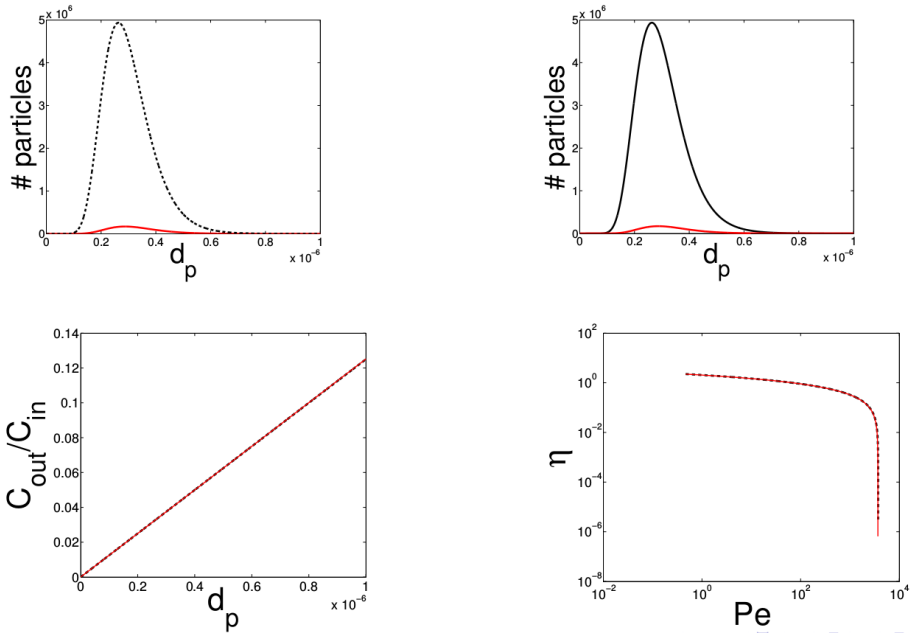

Figure A.14: Application of EQMOM (2 nodes) in the case of "linear" removal. On the top left the inlet distribution (dashed black line) and the theoretical expected distribution at the outlet (continuous red line). On the top right, the resulting EQMOM reconstructed curve (continuous red line). On the bottom, the theoretical expected results (black lines) and reconstructed results (red lines) calculating inlet-outlet concentration ratio (left) and deposition efficiency (right).

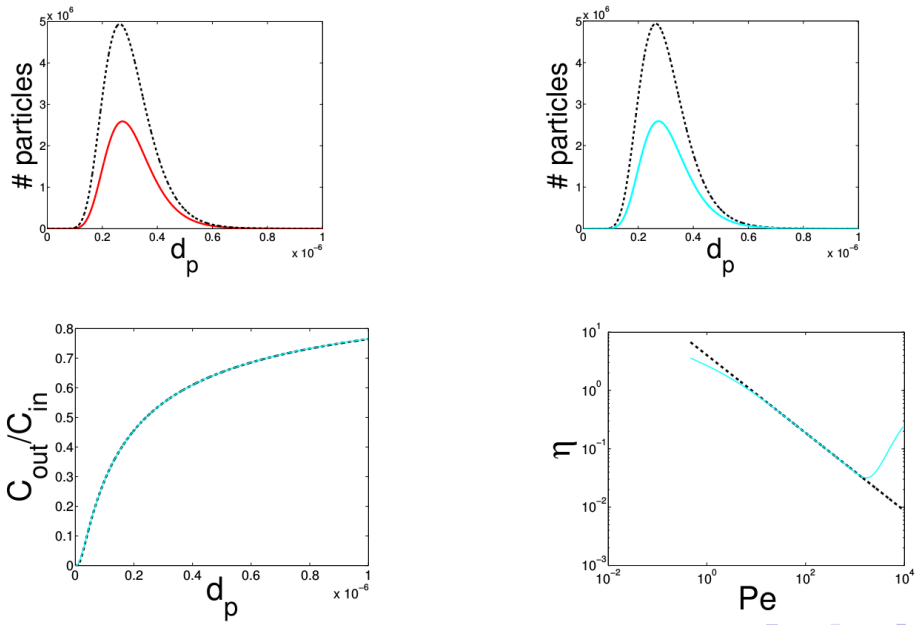

Figure A.15: Application of EQMOM (4 nodes) in the case of "packed bed filtration" removal. On the top left the inlet distribution (dashed black line) and the theoretical expected distribution at the outlet (continuous red line). On the top right, the resulting EQMOM reconstructed curve (continuous blue line). On the bottom, the theoretical expected results (black lines) and reconstructed results (blue lines) calculating inlet-outlet concentration ratio (left) and deposition efficiency (right).